Pairing and continuum effects on low-frequency quadrupole vibrations in deformed Mg isotopes close to the neutron drip line

K. Yoshida [a], M. Yamagami [b] and K. Matsuyanagi [a]

[a] *Department of Physics, Graduate School of Science, Kyoto University, Kyoto 606-8502, Japan*

[b] *Radioactive Isotope Physics Laboratory, RIKEN, Wako Saitama 351-0198, Japan*

Abstract

Low-frequency quadrupole vibrational modes in deformed ^{36,38,40}Mg close to the neutron drip line are studied by means of the quasiparticle-random-phase approximation based on the coordinate-space Hartree-Fock-Bogoliubov formalism. Strongly collective $K^\pi = 0^+$ and 2^+ excitation modes carrying $10 - 20$ Weisskopf units in the intrinsic isoscalar quadrupole transition strengths are obtained at about 3 MeV. There are two reasons for the enhancement of the transition strengths. First, the quasiparticle wave functions generating these modes possess spatially very extended structure. The asymptotic selection rules characterizing the β and γ vibrations in stable deformed nuclei are thus strongly violated. Second, the dynamic pairing effects act strongly to enhance the collectivity of these modes. It is suggested that the lowest $K^\pi = 0^+$ collective mode is a particularly sensitive indicator of the nature of pairing correlations in deformed nuclei close to the neutron drip line.

Key words: Hartree-Fock-Bogoliubov method, Quasiparticle-RPA, Collective excitations, Deformed unstable nuclei, Neutron drip line, Mg isotopes
PACS: 21.60.Ev, 21.60.Jz, 21.10.Re

1 Introduction

The physics of drip-line nuclei is one of the current frontiers in nuclear structure physics [1–3]. The number of unstable nuclei experimentally accessible will remarkably increase when the next generation of radioactive ion beam facilities start running. We shall be able to study the properties not only of the ground states but also of low-lying excited states of drip-line nuclei in

the medium-mass region. Collective excitation in neutron-rich nuclei is one of the most interesting issues in this field. Because properties of low-frequency collective vibrational modes are quite sensitive to surface effects and details of shell structure, we expect that new kinds of collective excitations emerge under such new situations of nuclear structure. In order to quest for collective modes of excitation unique to unstable nuclei associated with new features such as neutron skins, many attempts have been made using the self-consistent RPA based on the Skyrme-Hartree-Fock (SHF) method [4–6] and the Quasiparticle-RPA (QRPA) including the pairing correlations [7–12]. A number of similar approaches using different mean fields have also been carried out [14–22]. (See Refs. [12,19,23] for extensive lists of references concerning the self-consistent RPA and mean-field calculations.) Most of these calculations, however, are restricted to spherical nuclei.

Quite recently, low-frequency RPA modes in deformed nuclei close to the neutron drip line have been investigated by several authors. The time-dependent Hartree-Fock method formulated in the three-dimensional coordinate space with a complex absorbing boundary condition was applied to low-frequency isovector dipole modes [24]. Possible appearance of low-frequency octupole vibrations built on superdeformed states in neutron drip-line nuclei was discussed in Ref. [25] on the basis of the SHF plus mixed representation RPA [26–28] calculations. In Ref. [29], we investigated properties of octupole excitations built on superdeformed states in neutron-rich sulfur isotopes by means of the RPA based on the deformed Woods-Saxon (WS) potential in the coordinate-space mesh-representation. We found that low-lying states created by excitation of a single neutron from a loosely bound low-Ω state to a high-Ω resonance state (Ω being the z-component of the angular momentum) acquire extremely strong octupole transition strengths due to very extended spatial structure of particle-hole wave functions. All of these calculations, however, did not take into account the pairing correlation. In Refs. [30,31], low-lying Gamow-Teller β-decay strengths were investigated by means of the proton-neutron RPA using the SHF + BCS approximation. Gamma vibrations in ^{38}Mg were studied using the QRPA with the BCS approximation [32] on the basis of the response function formalism. It should be noted that these calculations relied on the BCS approximation, which is inappropriate, because of the unphysical nucleon gas problem [34], for describing continuum coupling effects in drip line nuclei.

The nature of pairing correlations in neutron drip-line nuclei is one of the most important subjects in the physics of unstable nuclei. One of the unique features of drip-line nuclei is that the pairing correlation takes place not only among bound levels but also including continuum states. To describe this unique character of pairing, the coordinate-space Hartree-Fock-Bogoliubov (HFB) formalism is suitable [33,34] and has been widely used for the study of single-particle motion and shell structure near the continuum [35–38]. Due to the pairing and continuum effects, spatial structure of quasiparticle wave functions near the

chemical potential changes significantly, which affects the properties of low-frequency excitation modes [39]. In order to study the effects of pairing on the low-frequency excitation modes in deformed nuclei near the neutron drip-line, we have extended the previous work to self-consistently include pairing correlations, and constructed a new computer code that carries out the deformed QRPA calculation on the basis of the coordinate-space HFB formalism.

The aim of this paper is to carry out the deformed QRPA calculation for neutron drip-line nuclei and investigate the low-frequency quadrupole vibrational modes with $K^\pi = 0^+$ and 2^+ in ^{36,38,40}Mg close to the neutron drip line. According to the Skyrme-HFB calculations [40,41] and Gogny-HFB calculation [42], these isotopes are well deformed. The shell-model calculation [43] also suggests that the ground state of ^{40}Mg is dominated by the neutron two-particle-two-hole components, which is consistent with the breaking of the $N = 28$ shell closure discussed in [44]. We investigate properties of low-frequency modes of excitation in these Mg isotopes simultaneously taking into account the deformed mean-field effects, the pairing correlations, and excitations into the continuum.

This paper is organized as follows: In the next section, the framework of the mean-field and QRPA calculations is briefly described. In Section 3, results of the RPA calculation for low-frequency quadrupole vibrations with $K^\pi = 0^+$ and 2^+ in ^{36,38,40}Mg are presented and discussed focusing our attention to the microscopic mechanism of emergence of collective modes in deformed superfluid nuclei close to the neutron drip line. Concluding remarks are given in §4.

A preliminary version of this work was previously reported in Ref. [45].

2 Method

2.1 Mean-field calculation

In order to discuss simultaneously effects of nuclear deformation and pairing correlations including the continuum, we solve the HFB equation [33,34,46]

$$\begin{pmatrix} h^\tau(\boldsymbol{r}\sigma) - \lambda^\tau & \tilde{h}^\tau(\boldsymbol{r}\sigma) \\ \tilde{h}^\tau(\boldsymbol{r}\sigma) & -(h^\tau(\boldsymbol{r}\sigma) - \lambda^\tau) \end{pmatrix} \begin{pmatrix} \varphi^\tau_{1,\alpha}(\boldsymbol{r}\sigma) \\ \varphi^\tau_{2,\alpha}(\boldsymbol{r}\sigma) \end{pmatrix} = E_\alpha \begin{pmatrix} \varphi^\tau_{1,\alpha}(\boldsymbol{r}\sigma) \\ \varphi^\tau_{2,\alpha}(\boldsymbol{r}\sigma) \end{pmatrix} \tag{1}$$

directly in the cylindrical coordinate space assuming axial and reflection symmetry. In comparison to the conventional method of using a deformed harmonic oscillator basis, this method is more effective in the treatment of spa-

tially extended wave functions, like loosely bound states, resonant states and continuum states. As is well known, when the quasiparticle energy E is greater than the absolute magnitude $|\lambda|$ of the chemical potential, the upper component $\varphi_1(\boldsymbol{r}\sigma)$ obeys the scattering-wave boundary condition, while the lower component $\varphi_2(\boldsymbol{r}\sigma)$ is always exponentially decaying at infinity.

For the mean-field Hamiltonian h, we employ the deformed Woods-Saxon potential with the parameters used in [29], except the isovector potential strength for which a slightly smaller value, 30 MeV in stead of 33 MeV, is adopted in order to describe ^{40}Mg as a drip-line nucleus in accordance with the Skyrme-HFB [40,41] and Gogny-HFB calculations [42]. The pairing field is treated self-consistently by using the density-dependent contact interaction [47,48],

$$v_{pp}(\boldsymbol{r},\boldsymbol{r}') = V_0\frac{1-P_\sigma}{2}\left[1-\eta\left(\frac{\varrho^{\rm IS}(\boldsymbol{r})}{\varrho_0}\right)\right]\delta(\boldsymbol{r}-\boldsymbol{r}'), \tag{2}$$

with $V_0 = -450$ MeV$\cdot$fm^3 and $\varrho_0 = 0.16$ fm^{-3}, where $\varrho^{\rm IS}(\boldsymbol{r})$ denotes the isoscalar density and P_σ is the spin exchange operator. The pairing force strength V_0 is chosen such that the average pairing gap roughly agrees with the systematics (see Table 1). For the parameter η, which represents density dependence, we use $\eta = 1.0$(surface type). Sensitivity of calculated results to the parameter η will be examined in subsection 3.4. The pairing Hamiltonian is then given by

$$\tilde{h}^\tau(\boldsymbol{r}) = \frac{V_0}{2}\left[1-\eta\left(\frac{\varrho^{\rm IS}(\boldsymbol{r})}{\varrho_0}\right)\right]\tilde{\varrho}^\tau(\boldsymbol{r}). \tag{3}$$

The normal and abnormal (pairing) densities are given by

$$\varrho^\tau(\rho,z) = \sum_\alpha \sum_{\sigma=\pm1/2} |\varphi^\tau_{2,\alpha}(\rho,z,\sigma)|^2, \tag{4}$$

$$\tilde{\varrho}^\tau(\rho,z) = -\sum_\alpha \sum_{\sigma=\pm1/2} \varphi^\tau_{1,\alpha}(\rho,z,\sigma)\varphi^\tau_{2,\alpha}(\rho,z,\sigma) \tag{5}$$

and the mean-square radii of protons and neutrons are calculated as

$$\langle r^2\rangle_\tau = \frac{\int \rho{\rm d}\rho{\rm d}z r^2\varrho^\tau(\rho,z)}{\int \rho{\rm d}\rho{\rm d}z\varrho^\tau(\rho,z)}, \tag{6}$$

where $\boldsymbol{r} = (\rho,z)$, $r = \sqrt{\rho^2+z^2}$ and τ=π or ν; $\varrho^\pi(\rho,z)$ and $\varrho^\nu(\rho,z)$ being the proton and neutron densities. The average gaps are defined by [49–52]

$$\langle\Delta_\tau\rangle = -\int {\rm d}\boldsymbol{r}\tilde{\varrho}^\tau(\boldsymbol{r})\tilde{h}^\tau(\boldsymbol{r})/\int {\rm d}\boldsymbol{r}\tilde{\varrho}^\tau(\boldsymbol{r}). \tag{7}$$

We construct the discretized Hamiltonian matrix by use of the finite difference method for derivatives and then diagonalize the matrix to obtain the

quasiparticle wave functions on the two-dimensional lattice consisting of the cylindrical coordinates ρ and z. The kinetic energy term and the spin-orbit potential are evaluated using the 9-point formula. Because the time-reversal symmetry and the reflection symmetry with respect to the $x-y$ plane are assumed, we have only to solve for positive Ω and positive z. We use the lattice mesh size $\Delta\rho = \Delta z = 0.8$ fm and the box boundary condition at $\rho_{\max} = 10.0$ fm and $z_{\max} = 12.8$ fm. The quasiparticle energy is cut off at 50 MeV and the quasiparticle states up to $\Omega^\pi = 13/2^\pm$ are included. This model space is larger than that used in Ref. [45]. It is certainly desirable to use a larger box for a better evaluation of matrix elements involving spatially very extended quasiparticle wave functions. This improvement remains as a future task, however.

We impose the condition on the convergence of the pairing energy as $|(E^{(i)}_{pair} - E^{(i-1)}_{pair})/E^{(i)}_{pair}| < 10^{-5}$, where i denotes the iteration number and the pairing energy is defined by [37]

$$E_{pair} = \frac{1}{2}\sum_{\tau=\pi,\nu}\int \mathrm{d}\boldsymbol{r}\,\tilde{\varrho}^\tau(\boldsymbol{r})\tilde{h}^\tau(\boldsymbol{r}). \tag{8}$$

We use the same deformation parameter $\beta_2 = 0.28$ in the Woods-Saxon potential for both neutrons and protons. This parameter is chosen to approximately reproduce the $Q-$moments calculated in Ref.[40]. We checked that properties of the QRPA modes do not change significantly when the deformation parameter is varied around $\beta_2 \sim 0.3$.

2.2 Quasiparticle-RPA calculation

Using the quasiparticle basis obtained in the previous subsection, we solve the QRPA equation in the standard matrix formulation [53]

$$\sum_{\gamma\delta}\begin{pmatrix} A_{\alpha\beta\gamma\delta} & B_{\alpha\beta\gamma\delta} \\ B_{\alpha\beta\gamma\delta} & A_{\alpha\beta\gamma\delta}\end{pmatrix}\begin{pmatrix} f^\lambda_{\gamma\delta} \\ g^\lambda_{\gamma\delta}\end{pmatrix} = \hbar\omega_\lambda \begin{pmatrix} 1 & 0 \\ 0 & -1\end{pmatrix}\begin{pmatrix} f^\lambda_{\alpha\beta} \\ g^\lambda_{\alpha\beta}\end{pmatrix}. \tag{9}$$

This method is convenient to analyze microscopic structures of the QRPA eigenmodes in comparison with other RPA formalisms based on the Greens function method. Namely, individual two-quasiparticle components, $(\alpha\beta)$, $(\gamma\delta)$, etc., constituting the QRPA mode λ are directly represented by the amplitudes $f^\lambda_{\gamma\delta}$ and $g^\lambda_{\gamma\delta}$, whereas an additional procedure is needed to obtain them in the latter method [54].

The residual interactions in the particle-particle channel appearing in the QRPA matrices A and B are self-consistently treated using the density-dependent

contact interaction (2). On the other hand, for residual interactions in the particle-hole channel, we use the Skyrme-type interaction [55]

$$v_{ph}(\boldsymbol{r},\boldsymbol{r}') = \left[t_0(1+x_0P_\sigma) + \frac{t_3}{6}(1+x_3P_\sigma)\varrho^{\rm IS}(\boldsymbol{r})\right]\delta(\boldsymbol{r}-\boldsymbol{r}'), \tag{10}$$

with $t_0 = -1100$ MeV·fm^3, $t_3 = 16000$ MeV·fm^6, $x_0 = 0.5$, and $x_3 = 1.0$. Because the deformed Wood-Saxon potential is used for the mean-field, we renormalize the residual interaction in the particle-hole channel by multiplying a factor f_{ph} to get the spurious $K^\pi = 1^+$ mode (representing the rotational mode) at zero energy ($v_{ph} \to f_{ph}\cdot v_{ph}$). This factor is found to be 0.380, 0.376 and 0.374 for ^{36}Mg, ^{38}Mg, and ^{40}Mg, respectively. It is desirable to carry out the QRPA calculation by using a model space which is consistent with that adopted in the HFB calculation. It requires, however, excessively demanding computer memory, so that we cut the model space by $E_\alpha + E_\beta \leq 30$ MeV. Accordingly, we need another self-consistency factor f_{pp} for the particle-particle channel. We determine this factor such that the spurious $K^\pi = 0^+$ mode associated with the number fluctuation appears at zero energy ($v_{pp} \to f_{pp}\cdot v_{pp}$). This factor is found to be 1.536 for $^{36-40}$Mg. The dimension of the QRPA matrix is about 3700 for the $K^\pi = 0^+$ modes in ^{40}Mg. We checked accuracy of the numerical calculation by applying our procedure to quadrupole excitations of the spherical nucleus ^{24}O and comparing the result with that of the continuum QRPA calculation by Matsuo[7] which exactly fulfils the energy-weighted sum-rule. It turned out that, although the overall structure of the strength distribution was well reproduced, the energy-weighted sum-rule value was underestimated by 14% due to the truncation of the model space. This shortcoming should be overcome in future by enlarging the QRPA model space.

In terms of the nucleon annihilation and creation operators in the coordinate representation, $\hat\psi(\boldsymbol{r}\sigma)$ and $\hat\psi^\dagger(\boldsymbol{r}\sigma)$, the quadrupole operator is represented as $\hat Q_{2K} = \sum_\sigma \int {\rm d}\boldsymbol{r} r^2 Y_{2K}(\hat r)\hat\psi^\dagger(\boldsymbol{r}\sigma)\hat\psi(\boldsymbol{r}\sigma)$. The intrinsic matrix elements $\langle\lambda|\hat Q_{2K}|0\rangle$ of the quadrupole operator between the excited state $|\lambda\rangle$ and the ground state $|0\rangle$ are given by

$$\langle\lambda|\hat Q_{2K}|0\rangle = \sum_{\alpha\beta} Q^{\rm (uv)}_{2K,\alpha\beta}(f^\lambda_{\alpha\beta} + g^\lambda_{\alpha\beta}) = \sum_{\alpha\beta} M^{\rm (uv)}_{2K,\alpha\beta}, \tag{11}$$

where

$$Q^{\rm (uv)}_{2K,\alpha\beta} \equiv 2\pi\delta_{K,\Omega_\alpha+\Omega_\beta}\int {\rm d}\rho{\rm d}z Q^{\rm (uv)}_{2K,\alpha\beta}(\rho,z), \tag{12}$$

with

$$\begin{aligned} Q^{\rm (uv)}_{2K,\alpha\beta}(\rho,z) = \rho\{&\varphi_{1,\alpha}(\rho,z,\downarrow)\varphi_{2,\beta}(\rho,z,\uparrow) - \varphi_{1,\alpha}(\rho,z,\uparrow)\varphi_{2,\beta}(\rho,z,\downarrow) \\ &- \varphi_{1,\beta}(\rho,z,\downarrow)\varphi_{2,\alpha}(\rho,z,\uparrow) + \varphi_{1,\beta}(\rho,z,\uparrow)\varphi_{2,\alpha}(\rho,z,\downarrow)\}Q_{2K}(\rho,z). \end{aligned} \tag{13}$$

Here $Q_{2K}(\rho, z) = Q_{2K}(\boldsymbol{r})e^{-iK\varphi} = r^2 Y_{2K}(\theta, \varphi)e^{-iK\varphi}$.

We calculate the transition strength functions

$$S^{\rm IS}(\omega) = \sum_{\lambda} |\langle\lambda|\hat{Q}^{\rm IS}_{2K}|0\rangle|^2 \delta(\hbar\omega - \hbar\omega_\lambda) \tag{14}$$

for isoscalar quadrupole operators $\hat{Q}^{\rm IS}_{2K} = \hat{Q}^{\pi}_{2K} + \hat{Q}^{\nu}_{2K}$, and use notations $B(Q^\tau 2) = |\langle\lambda|\hat{Q}^{\tau}_{2K}|0\rangle|^2$ for transition strengths and $M_\tau = \langle\lambda|\hat{Q}^{\tau}_{2K}|0\rangle$ for transition matrix elements ($\tau = \pi, \nu$, IS). Note that these quantities are defined in the intrinsic coordinate frame associated with the deformed mean field, so that appropriate Clebsh-Gordan coefficients should be multiplied to obtain transition probabilities in the laboratory frame [56]. For instance, a factor 1/5 should be multiplied for obtaining the transition strength $B(E2; 2^+_1 \to 0^+_\beta)$ from the 2^+_1 state to the 0^+_β state, while the factor is unity for obtaining the transition strength $B(E2; 0^+_{\rm gs} \to 2^+_\beta)$ from the ground state to the 2^+_β state built on the excited $K^\pi = 0^+$ state. Here, 2^+_1 denotes the 2^+ member of the ground-state rotational band, while 0^+_β and 2^+_β indicate the rotational band members associated with the $K^\pi = 0^+$ intrinsic excitations.

3 Results and Discussion

3.1 Some features of calculated results

The single-particle shell structure around the Fermi surface for neutrons in ^{36,38,40}Mg exhibits an interesting feature. Figure 1 shows the single-particle energy diagram for the WS potential as functions of deformation parameter β_2. As β_2 increases, a level crossing between the up-sloping [303]7/2 level and the down-sloping [310]1/2 level takes place, and a deformed shell gap is formed at $N = 28$ around $\beta_2 = 0.3$. This deformed closed shell approximately corresponds to the $(f_{7/2})^{-2}(p_{3/2})^2$ configuration in the spherical shell model representation. The highest occupied level in this deformed closed shell is situated very near to the continuum threshold, so that there is no bound level above it. However, neutron particle-hole excitations may take place into resonance levels like [303]7/2, [301]1/2 [312]3/2 lying just above the continuum threshold. In fact, as we shall discuss below, these resonance levels participate in the pairing correlations and play an important role in generating low-frequency collective modes of excitation in ^{36,38,40}Mg. Thus, ^{40}Mg and its neighboring isotopes provide an interesting situation to investigate collective modes unique in unstable nuclei near the neutron drip line. The resonance character of these levels just above the continuum threshold is confirmed by means of the eigenphase-sum method (see Appendix).

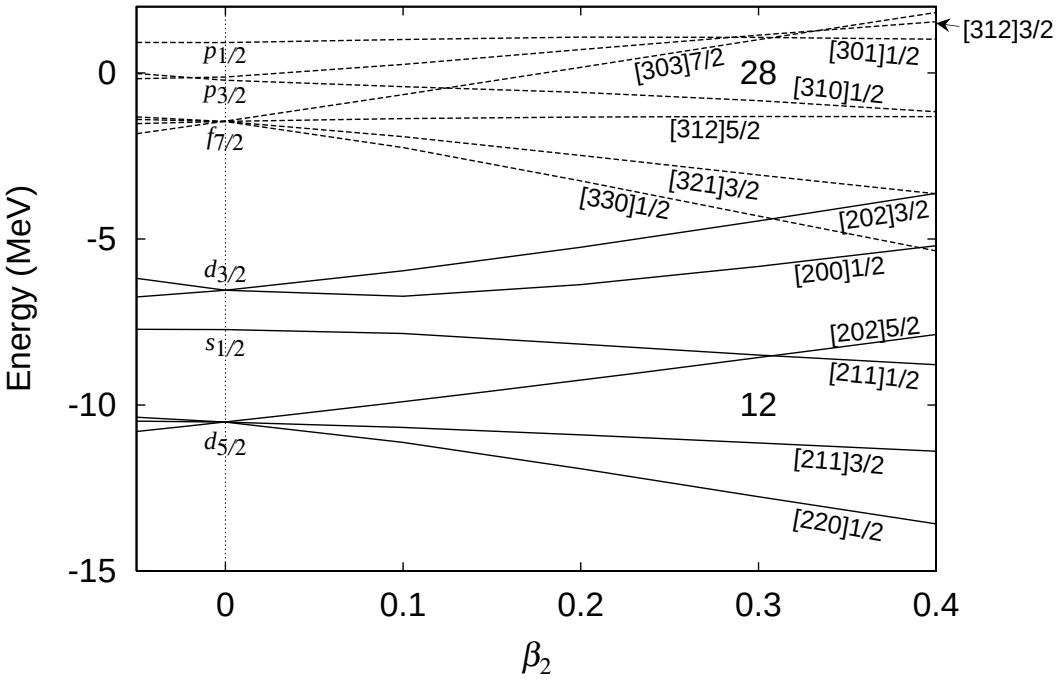

Fig. 1. Single-particle energies in the deformed WS potential for neutrons in ^{40}Mg, plotted as functions of the quadrupole deformation parameter β_2. Solid and dotted lines denote positive- and negative-parity levels, respectively. Single-particle levels are labeled with the asymptotic quantum numbers $[Nn_3\Lambda]\Omega$.

Table 1
Ground state properties of ^{36,38,40}Mg obtained by the deformed WS-HFB calculation with $\beta_2 = 0.28$. Chemical potentials, average pairing gaps, and root-mean-square radii for protons and neutrons are listed.

nucleus	λ_π (MeV)	$\overline{\Delta}_\pi$ (MeV)	$\sqrt{\langle r^2\rangle_\pi}$ (fm)	λ_ν (MeV)	$\overline{\Delta}_\nu$ (MeV)	$\sqrt{\langle r^2\rangle_\nu}$ (fm)
^{36}Mg	−20.0	0.0	3.06	−2.09	1.93	3.74
^{38}Mg	−23.0	0.0	3.08	−1.15	2.05	3.86
^{40}Mg	−25.1	0.0	3.10	−0.41	2.15	3.99

Results of the deformed WS plus HFB calculation for the ground state properties of ^{36,38,40}Mg are listed in Table 1. Calculated values of the average pairing gap for neutrons are rather close to the value estimated in terms of the conventional systematics [57] $\Delta_{\rm syst} \simeq 12/\sqrt{A} \simeq 1.9$MeV. On the other hand, the average pairing gaps for protons vanish. As shown in this table, the neutron root-mean-square radius increases as approaching the neutron drip line, while the proton root-mean-square radius remains almost constant. This means that the neutron skin structure emerges in these nuclei; the difference between the neutron and proton radii in ^{40}Mg is about 0.9 fm.

Results of the QRPA calculation for quadrupole transition strengths are dis-

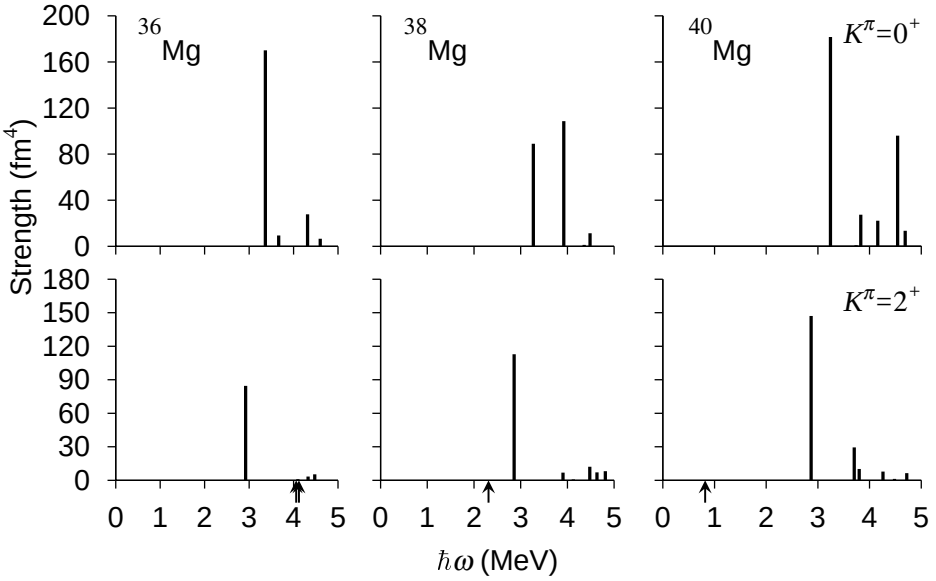

Fig. 2. Isoscalar quadrupole transition strengths $B(Q^{\rm IS}2)$ for the $K = 0^+$ excitations (upper panel) and the $K = 2^+$ excitations (lower panel) built on the prolately deformed ground states of ^{36,38,40}Mg. The arrows beside the abscissa axes indicate the neutron threshold energies, $E_{\rm th} = 4.06$ MeV (one-quasiparticle (1qp) continuum; $|\lambda| + \min E_\alpha$), 4.12 MeV (two quasiparticle (2qp) continuum; $2|\lambda|$) for ^{36}Mg, 2.31 MeV (2qp continuum) for ^{38}Mg and 0.82 MeV (2qp continuum) for ^{40}Mg. The QRPA calculations are made by using the surface-type pairing interaction and $\beta_2 = 0.28$ for both protons and neutrons.

played in Fig. 2. We see prominent peaks at about 3 MeV for both the $K^\pi = 0^+$ and 2^+ excitations. Their strengths are much larger than the single-particle strengths indicating collective character of these excitations. The strength of the lowest $K^\pi = 2^+$ excitation gradually increases as approaching the neutron drip line, while the lowest $K^\pi = 0^+$ excitations in ^{36}Mg and ^{40}Mg seem to be split into two peaks in the case of ^{38}Mg. In the following, we make an extensive analysis on microscopic structure of these low-frequency collective excitations.

3.2 $K^\pi = 0^+$ modes

We first discuss the $K^\pi = 0^+$ excitation modes in ^{40}Mg. The QRPA transition strengths are compared with unperturbed two-quasiparticle strengths in Fig. 3 . A prominent peak is seen at about 3.2 MeV in the QRPA strength distribution; it possesses an enhanced strength of about 22 Weisskopf unit (1 W.u. $\simeq 8.1$ fm^4 for ^{40}Mg). From the QRPA amplitudes listed in Table 2, it is clear that this collective mode is generated by coherent superposition of neutron excitations of both particle-hole and particle-particle types. In Fig. 3, the QRPA strengths are also compared with the strengths without the dynamical pairing effects, i.e., the result of QRPA calculation ignoring the residual pair-

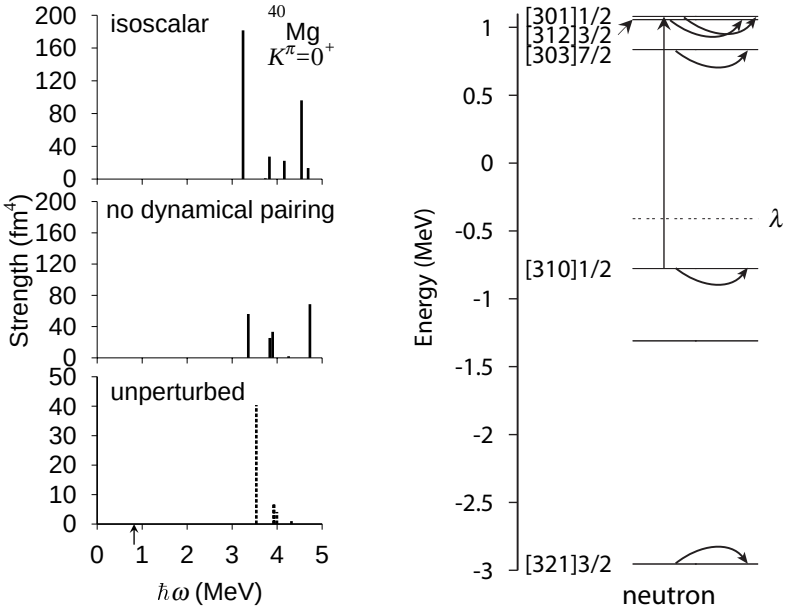

Fig. 3. *Left*: Isoscalar quadrupole transition strengths $B(Q^{\rm IS}2)$ for the $K^\pi = 0^+$ excitations in ^{40}Mg. Results of the QRPA calculation with and without including the dynamical pairing effects are plotted in the upper and middle panels, respectively, while unperturbed two-quasiparticle strengths are shown in the lower panel. Notice that different scale is used for the unperturbed strengths. The arrow beside the abscissa axis indicates the neutron threshold energy $2|\lambda| = 0.82$ MeV. *Right*: Two-quasiparticle excitations generating the lowest $K^\pi = 0^+$ mode at 3.2 MeV. The single-particle levels for the deformed WS potential are labeled with the asymptotic quantum numbers $[Nn_3\Lambda]\Omega$. The chemical potential λ is indicated by the dashed line.

Table 2
QRPA amplitudes of the $K^\pi = 0^+$ mode at 3.2 MeV in ^{40}Mg. This mode has $B(E2) = 3.4\ e^2{\rm fm}^4$, $B(Q^\nu 2)$=136 fm^4, and $B(Q^{\rm IS}2) = 182$ fm^4. The single-particle levels are labeled with the asymptotic quantum numbers $[Nn_3\Lambda]\Omega$ of the dominant components of the wave functions. Only components with $|f_{\alpha\beta}|^2 - |g_{\alpha\beta}|^2 > 0.01$ are listed.

	α	β	$E_\alpha + E_\beta$ (MeV)	$\lvert f_{\alpha\beta}\rvert^2 - \lvert g_{\alpha\beta}\rvert^2$	$Q^{(\rm uv)}_{20,\alpha\beta}$ (fm^2)	$M^{(\rm uv)}_{20,\alpha\beta}$ (fm^2)
(a)	ν[310]1/2	ν[310]1/2	3.54	0.438	6.36	4.27
(b)	ν[301]1/2	ν[310]1/2	3.93	0.067	−2.57	0.925
(c)	ν[312]3/2	ν[312]3/2	3.99	0.280	−2.03	1.08
(d)	ν[301]1/2	ν[301]1/2	4.32	0.027	0.992	−0.176
(e)	ν[303]7/2	ν[303]7/2	5.76	0.077	−3.39	0.966
(f)	ν[321]3/2	ν[321]3/2	7.15	0.011	3.23	0.396

ing interactions. One immediately notice that the transition strength to the lowest excited state is drastically reduced when the dynamical pairing effects are ignored.

Let us discuss the reason why the lowest $K^\pi = 0^+$ mode acquires eminently large transition strength. There are two points to understand this mechanism: 1) existence of unperturbed two-quasiparticle configurations possessing large transition strengths, and 2) effect of residual interactions producing coherence among various two-quasiparticle configurations.

To examine the first point, we plot in Fig. 4 spatial distributions of the quadrupole transition amplitudes for major two-quasiparticle configurations generating the lowest $K^\pi = 0^+$ mode. We see that they are notably extended beyond the half-density radius. This is a situation similar to that encountered in Ref. [29], where a neutron excitation from a loosely bound state to a resonance state brings about very large transition strength. We also note that the transition strength associated with the $\nu[301]1/2 \otimes \nu[310]1/2$ configuration is much enhanced although it should be hindered if the selection rule $\Delta N = 2$ for the asymptotic quantum numbers [56] is applied. This selection rule is broken for matrix elements associated with loosely bound states, because their radial wave functions are spatially extended and quite different from those of the the harmonic oscillator potential.

Concerning the second point, we have found that the dynamical pairing plays an especially important role. This point is easily seen by comparing the QRPA calculations with and without the dynamical pairing effects, which are shown in Fig. 3. It is apparent that the prominent lowest peak disappears when the dynamical paring effects are ignored. We can say that the coherent superpositions among the particle-hole, particle-particle and hole-hole excitations are indispensable for the emergence of this mode. The importance of the coupling between the (particle-hole type) β vibration and the (particle-particle and hole-hole type) pairing vibration has been well known in stable deformed nuclei [56]. A new feature of the $K^\pi = 0^+$ mode in neutron drip-line nuclei under discussion is that this coupling takes place among two-quasiparticle configurations that are loosely bound or resonances, so that their transition strengths are strikingly enhanced. In addition, as seen in Fig. 4, their spatial structures (peak positions and distribution) are rather similar with each other. This is a favorable situation to generates coherence among them [39]. The importance of dynamical pairing effects in generating soft dipole excitations has been demonstrated by Matsuo et al. [13] for spherical unstable nuclei near the neutron drip line.

Next we discuss the $K^\pi = 0^+$ excitations in ^{38}Mg and ^{36}Mg. The quadrupole transition strengths calculated for ^{38}Mg are presented in Fig. 5, which exhibits two peaks below 4 MeV. The major two-quasiparticle excitations generating

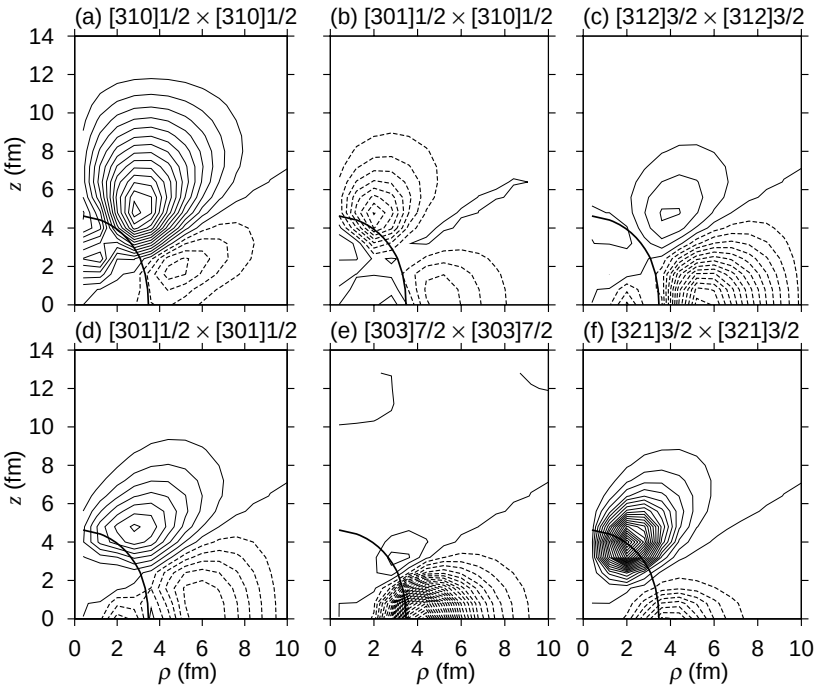

Fig. 4. Spatial distribution functions $Q^{(\mathrm{uv})}_{20,\alpha\beta}(\rho, z)$ for some two-quasiparticle excitations generating the lowest $K^\pi = 0^+$ mode in ^{40}Mg. The contour lines are plotted at intervals of 0.002. The solid and dashed lines represent positive and negative quantities, respectively. The thick solid line indicates the neutron half-density radius; $\varrho_\nu(0)/2 \sim 0.045\mathrm{fm}^{-3}$.

Table 3
QRPA amplitudes of the $K^\pi = 0^+$ mode at 3.3 MeV in ^{38}Mg. This mode has $B(E2) = 1.67\ e^2\mathrm{fm}^4$, $B(Q^\nu 2)$=66.3 fm^4, $B(Q^{\mathrm{IS}}2)$=89.0 fm^4, and $\sum |g_{\alpha\beta}|^2 = 2.32 \times 10^{-2}$. Only components with $|f_{\alpha\beta}|^2 - |g_{\alpha\beta}|^2 > 0.01$ are listed.

	α	β	$E_\alpha + E_\beta$ (MeV)	$\lvert f_{\alpha\beta}\rvert^2 - \lvert g_{\alpha\beta}\rvert^2$	$Q^{(\mathrm{uv})}_{20,\alpha\beta}$ (fm^2)	$M^{(\mathrm{uv})}_{20,\alpha\beta}$ (fm^2)
(a)	ν[310]1/2	ν[310]1/2	3.37	0.673	6.08	5.25
(b)	ν[312]5/2	ν[312]5/2	4.84	0.146	0.821	−0.293
(c)	ν[310]1/2	ν[330]1/2	5.35	0.023	−3.59	0.769
(d)	ν[303]7/2	ν[303]7/2	6.35	0.066	−2.64	0.614
(e)	ν[202]3/2	ν[202]3/2	7.82	0.021	−1.29	0.149

these peaks are illustrated in the middle and right panels of this figure. Their QRPA amplitudes are listed in Tables 3 and 4. From these Tables, it is seen that the peak at 3.3 MeV is mainly generated by the particle-particle type $\nu[310]1/2 \otimes \nu[310]1/2$ and $\nu[312]5/2 \otimes \nu[312]5/2$ excitations, while the peak at 3.9 MeV is mainly associated with the particle-hole type $\nu[301]1/2 \otimes \nu[310]1/2$ and $\nu[312]3/2 \otimes \nu[321]3/2$ excitations.

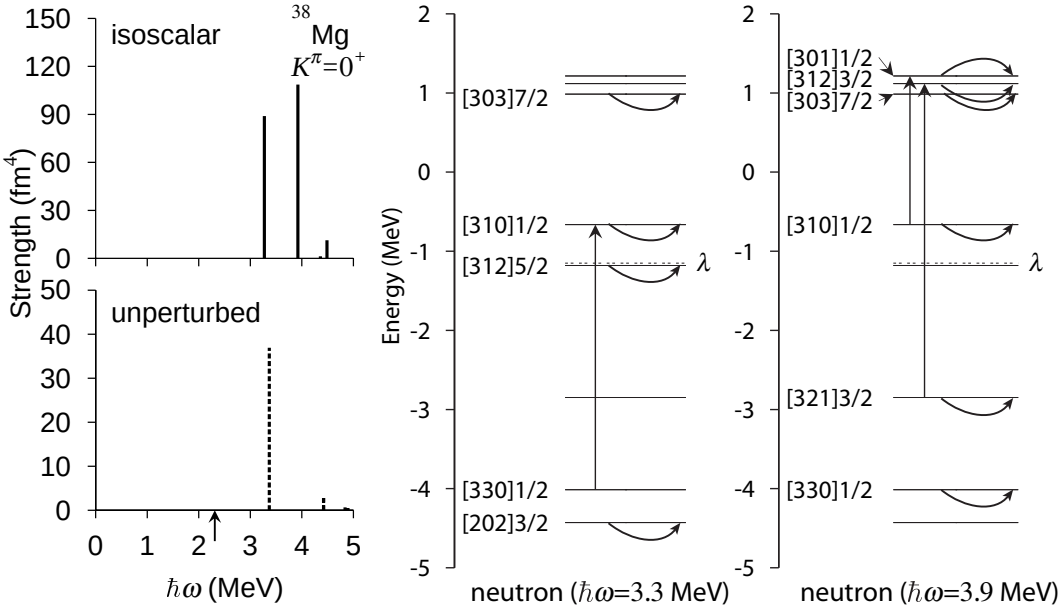

Fig. 5. *Left*: Isoscalar quadrupole transition strengths $B(Q^{\rm IS}2)$ for the $K^\pi = 0^+$ excitations in ^{38}Mg are plotted in the upper panel, while unperturbed two-quasiparticle strengths are shown in the lower panel. The arrow beside the abscissa axis indicates the neutron threshold energy $2|\lambda| = 2.31$ MeV. *Right*: Two-quasiparticle excitations generating the low-lying $K^\pi = 0^+$ modes at 3.3 MeV and 3.9 MeV.

Table 4
QRPA amplitudes of the $K^\pi = 0^+$ mode at 3.9 MeV in ^{38}Mg. This mode has $B(E2) = 4.72\ e^2$fm^4, $B(Q^\nu 2)$=68.1 fm^4, $B(Q^{\rm IS}2)$=109 fm^4, and $\sum|g_{\alpha\beta}|^2 = 2.71 \times 10^{-2}$. Only components with $|f_{\alpha\beta}|^2 - |g_{\alpha\beta}|^2 > 0.01$ are listed.

	α	β	$E_\alpha + E_\beta$ (MeV)	$\lvert f_{\alpha\beta}\rvert^2 - \lvert g_{\alpha\beta}\rvert^2$	$Q^{(\rm uv)}_{20,\alpha\beta}$ (fm^2)	$M^{(\rm uv)}_{20,\alpha\beta}$ (fm^2)
(a)	ν[310]1/2	ν[310]1/2	3.37	0.037	6.08	1.34
(b)	ν[301]1/2	ν[310]1/2	4.42	0.258	1.67	−1.20
(c)	ν[312]3/2	ν[312]3/2	4.90	0.048	0.716	0.169
(d)	ν[312]3/2	ν[321]3/2	5.47	0.250	−3.04	−2.20
(e)	ν[301]1/2	ν[301]1/2	5.47	0.018	0.802	0.131
(f)	ν[321]3/2	ν[321]3/2	6.04	0.058	1.66	−0.411
(g)	ν[303]7/2	ν[303]7/2	6.35	0.084	−2.64	−0.853
(h)	ν[330]1/2	ν[330]1/2	7.33	0.099	4.57	−1.48

The quadrupole transition strengths calculated for ^{36}Mg are displayed in Fig. 6. We notice a prominent peak at about 3.4 MeV below the one-neutron threshold energy (4.1 MeV), which possesses a strongly enhanced transition strength of about 24 W.u. (1 W.u. $\simeq$ 7.1 fm^4 for ^{36}Mg). This peak exhibits

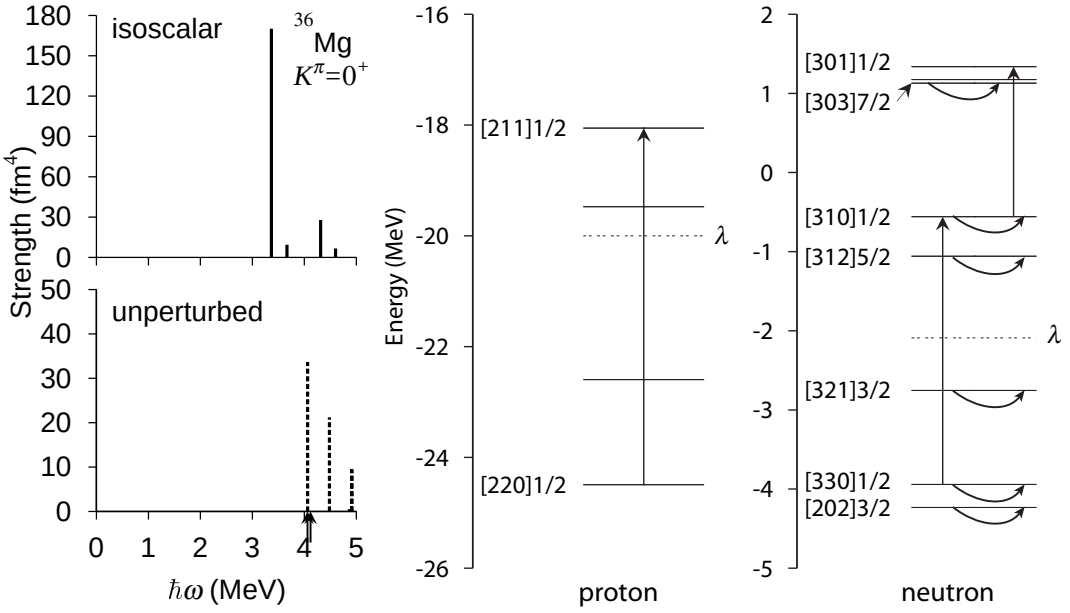

Fig. 6. *Left*: Isoscalar quadrupole transition strengths $B(Q^{\rm IS}2)$ for the $K^\pi = 0^+$ excitations in ^{36}Mg are plotted in the upper panel, while unperturbed two-quasiparticle strengths are shown in the lower panel. The arrows beside the abscissa axis indicate the neutron threshold energy $E_{\rm th} = 4.06$ MeV (1qp continuum) and 4.12 MeV (2qp continuum). *Right*: Two-quasiparticle excitations generating the lowest $K^\pi = 0^+$ mode at 3.4 MeV in ^{36}Mg.

Table 5
QRPA amplitudes of the $K^\pi = 0^+$ mode at 3.4 MeV in ^{36}Mg. This mode has $B(E2) = 8.1\ e^2{\rm fm}^4$, $B(Q^\nu 2)$=104 fm^4, $B(Q^{\rm IS}2)$=170 fm^4, and $\sum |g_{\alpha\beta}|^2 = 3.91 \times 10^{-2}$. Only components with $|f_{\alpha\beta}|^2 - |g_{\alpha\beta}|^2 > 0.01$ are listed.

	α	β	$E_\alpha + E_\beta$ (MeV)	$\lvert f_{\alpha\beta}\rvert^2 - \lvert g_{\alpha\beta}\rvert^2$	$Q^{(\rm uv)}_{20,\alpha\beta}$ (fm^2)	$M^{(\rm uv)}_{20,\alpha\beta}$ (fm^2)
(a)	ν[310]1/2	ν[310]1/2	4.06	0.071	5.80	−1.58
(b)	ν[321]3/2	ν[321]3/2	4.48	0.098	4.60	−1.61
(c)	ν[312]5/2	ν[312]5/2	4.87	0.227	0.714	0.347
(d)	ν[310]1/2	ν[330]1/2	4.91	0.211	−3.08	−2.11
(e)	ν[301]1/2	ν[310]1/2	5.69	0.033	2.02	−0.511
(f)	ν[330]1/2	ν[330]1/2	5.76	0.116	3.98	−1.50
(g)	ν[202]3/2	ν[202]3/2	5.79	0.046	−1.47	−0.271
(h)	ν[303]7/2	ν[303]7/2	7.67	0.049	−1.82	−0.411
(i)	π[211]1/2	π[220]1/2	6.44	0.054	−0.251	-0.599

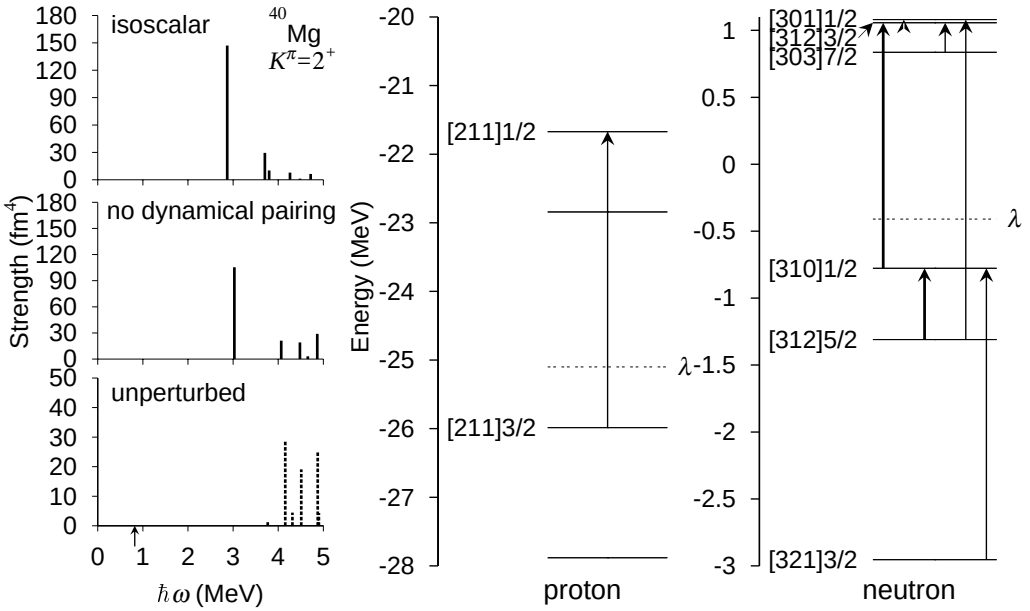

Fig. 7. *Left*: Isoscalar quadrupole transition strengths $B(Q^{\rm IS}2)$ for the $K^\pi = 2^+$ excitations in ^{40}Mg. Results of the QRPA calculation with and without including the dynamical pairing effects are plotted in the upper and middle panels, respectively, while unperturbed two-quasiparticle strengths are shown in the lower panel. Notice that different scale is used for the unperturbed strengths. The arrow beside the abscissa axis indicates the neutron threshold energy $2|\lambda| = 0.82$ MeV. *Right*: Two-quasiparticle excitations generating the lowest $K^\pi = 2^+$ mode at 2.9 MeV. Two-quasiparticle excitations satisfying the asymptotic selection rule for the γ vibration ($\Delta N = 0, \Delta n_3 = 0, \Delta\Lambda = 2$) are drawn by thick arrows.

a clear character of collective vibration: As seen from Table 5, this collective mode is created by coherent neutron excitations. Its main components are the particle-hole type $\nu[310]1/2 \otimes \nu[330]1/2$ and $\nu[301]1/2 \otimes \nu[310]1/2$ excitations and the particle-particle type $\nu[312]5/2 \otimes \nu[312]5/2$ and $\nu[321]3/2 \otimes \nu[321]3/2$ excitations. These particle-particle type and particle-hole type excitations are coherently superposed to generate this collective neutron mode.

3.3 $K^\pi = 2^+$ modes

Let us now turn to the $K^\pi = 2^+$ excitation modes. The quadrupole transition strengths calculated for ^{40}Mg are displayed in Fig. 7. We notice a prominent peak at about 2.8 MeV which possesses strongly enhanced transition strength of about 19 W.u. The QRPA amplitudes of this excitation are listed in Table 6. From this Table, we see that this peak represents a collective excitation consisting of a coherent superposition of the proton particle-hole excitation from the [211]3/2 level to the [211]1/2 level and a number of neutron two-quasiparticle excitations. Similarly to the $K^\pi = 0^+$ excitation modes discussed

Table 6
QRPA amplitudes of the $K^\pi = 2^+$ mode at 2.9 MeV in ^{40}Mg. This mode has $B(E2) = 11.7\ e^2\mathrm{fm}^4$, $B(Q^\nu 2)$=75.7 fm^4, $B(Q^{\mathrm{IS}}2)$=147 fm^4, and $\sum |g_{\alpha\beta}|^2 = 6.73 \times 10^{-2}$. Only components with $|f_{\alpha\beta}|^2 - |g_{\alpha\beta}|^2 > 0.01$ are listed. The label $\nu 1/2^-$ denotes a discretized non-resonant continuum state.

	α	β	$E_\alpha + E_\beta$ (MeV)	$\lvert f_{\alpha\beta}\rvert^2 - \lvert g_{\alpha\beta}\rvert^2$	$Q^{(\mathrm{uv})}_{22,\alpha\beta}$ (fm^2)	$M^{(\mathrm{uv})}_{22,\alpha\beta}$ (fm^2)
(a)	ν[312]3/2	ν[310]1/2	3.77	0.013	1.22	−0.145
(b)	ν[301]1/2	ν[312]3/2	4.16	0.098	−5.37	−1.75
(c)	ν[310]1/2	ν[312]5/2	4.51	0.085	−4.37	−1.34
(d)	ν[312]3/2	ν[303]7/2	4.88	0.011	−5.03	−0.454
(e)	ν[301]1/2	ν[312]5/2	4.90	0.016	−2.07	−0.296
(f)	ν[310]1/2	ν[321]3/2	5.34	0.047	−2.67	−0.663
(g)	$\nu 1/2^-$	ν[312]5/2	6.96	0.015	1.93	−0.298
(h)	$\nu 1/2^-$	ν[321]3/2	7.28	0.018	1.46	−0.265
(i)	π[211]1/2	π[211]3/2	4.32	0.596	−2.11	−2.02

in the previous subsection, the asymptotic selection rule ($\Delta N = 0, \Delta n_3 = 0, \Delta\Lambda = 2$) well known for the γ vibrations [56] is violated for the neutron excitations, because these levels are loosely bound or resonances and their quasiparticle wave functions are significantly extended outside of the nucleus. On the other hand, proton particle-hole excitations satisfy the selection rule because they are deeply bound. We also show in Fig. 7 the result of QRPA calculation where the residual pairing interaction is turned off. Comparing with the full QRPA result, we see that the transition strength is reduced about 30%. Thus, the dynamical pairing effect is important, though its effect is weaker than for the $K^\pi = 0^+$ mode. This is because the $K^\pi = 2^+$ mode consists of both proton and neutron excitations and the pairing is effective only for neutrons.

For ^{36,38}Mg, we also obtained a prominent peak at about 2.9 MeV which possesses strongly enhanced transition strength (about 15 W.u. and 12 W.u. for ^{38}Mg and ^{36}Mg, respectively) as shown in Fig. 2. These modes possess essentially the same microscopic structure as the collective $K^\pi = 2^+$ mode in ^{40}Mg discussed above. They also correspond to the γ vibrational mode obtained in the previous QRPA calculation[32] for ^{38}Mg. In our calculation, however, the collectivity of these modes remains almost the same even if we use different deformations for protons and neutrons, differently from Ref. [32].

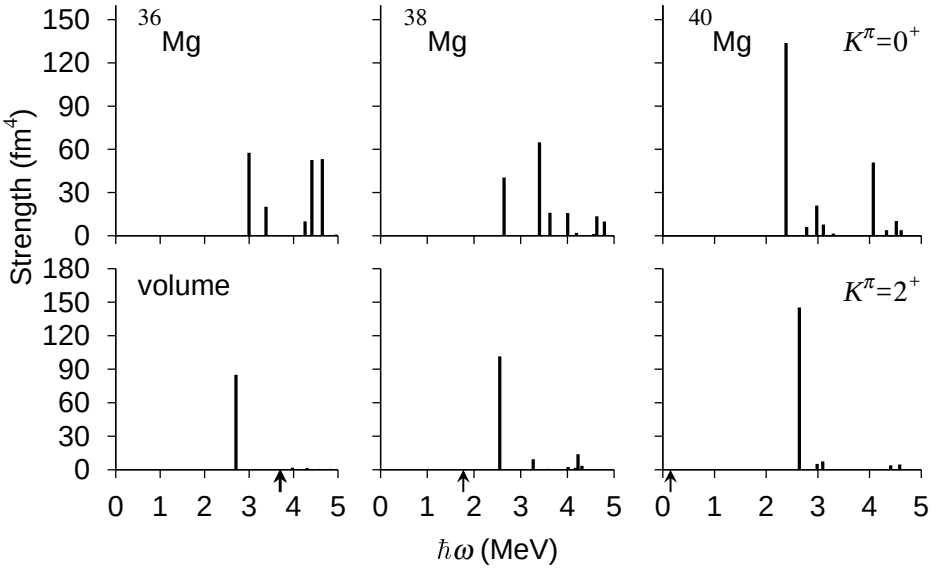

Fig. 8. Isoscalar quadrupole transition strengths $B(Q^{\rm IS}2)$ for the $K = 0^+$ excitations (upper panel) and the $K = 2^+$ excitations (lower panel) built on the prolately deformed ground states of ^{36,38,40}Mg. The QRPA calculations are made in the same way as in Fig. 2, except that the volume-type pairing interaction is used here. The arrows indicate the neutron threshold energies; 3.69 MeV (1qp continuum) and 3.71 MeV (2qp continuum) for ^{36}Mg, 1.77 MeV (2qp continuum) for ^{38}Mg, and 0.15 MeV (2qp continuum) for ^{40}Mg.

3.4 Dependence on pairing interaction

In this subsection, we examine sensitivity of the low-frequency $K^\pi = 0^+$ and 2^+ modes on the density dependence of the pairing interaction. For this purpose, we repeated the HFB and QRPA calculations using pairing interactions with density dependence different from the surface type ($\eta = 1.0$ in Eq. (2)); i.e., the mixed type ($\eta = 0.5$) and the volume type ($\eta = 0.0$). Since the result for the mixed-type pairing is intermediate between those for the surface-type and the volume-type, we show in Fig. 8 only the quadrupole transition strengths obtained using the volume-type pairing interaction. In this calculation, the pairing interaction strength $V_0 = -215.0$ MeV·fm^3 is chosen to yield approximately the same average pairing gaps as those for the surface type. Comparing with the results obtained using the surface-type pairing, shown in Fig. 2, we see that the transition strengths for the $K^\pi = 0^+$ collective modes are appreciably reduced, while those for the $K^\pi = 2^+$ collective modes are almost the same. We have checked that, although the strengths are reduced, the microscopic structure of these collective modes are basically the same as discussed above on the basis of the results of calculation using the surface-type pairing interaction. Thus, we can say that the quadrupole transition strengths for the low-frequency $K^\pi = 0^+$ collective modes are especially sensitive to the density dependence of the pairing interaction. Such a sensitivity has been stressed

also in Refs. [7,10,13] in their continuum QRPA calculations for $E1$ and $E2$ strength functions in neutron rich spherical nuclei.

4 Concluding remarks

We have carried out the QRPA calculations on the basis of the deformed WS plus HFB mean field in the coordinate representation, and obtained the low-frequency $K^\pi = 0^+$ and 2^+ collective modes in deformed ^{36,38,40}Mg close to the neutron drip line. It has been shown that these modes possess very strong isoscalar quadrupole transition strengths. One of the reasons of this enhancement is that the quasiparticle wave functions participating in these collective excitations have spatially extended structure. The other reason is that the residual pairing interactions, in addition to the particle-hole type residual interactions, enhance the collectivity of these modes. The result of the present calculation suggests that the low-frequency $K^\pi = 0^+$ collective mode is a particularly sensitive indicator of the nature of pairing correlations in nuclei close to the neutron drip line.

This paper should be regarded as an exploratory work toward understanding low-frequency collective modes of excitation in unstable nuclei close to the neutron drip line. It is certainly desirable to improve the treatment of the continuum at least in the following points. First, one may try to use a smaller mesh size and a larger box by implementing an adaptive coordinate method[24]. Second, one may try to take into account the width of resonance by employing Gamow states as basis of the QRPA calculation[62]. The result of the present work indicates that calculations using such an improved framework will be very interesting and worthwhile. We plan to attack this subject in future.

Acknowledgment

This work was done as a part of the Japan-U.S. Cooperative Science Program "Mean-Field Approach to Collective Excitations in Unstable Medium-Mass and Heavy Nuclei" during the academic year 2003-2004, and we acknowledge useful discussions with the member of this project. This work was also supported by the JSPS Core-to-Core Program "International Research Network for Exotic Femto Systems." One of the authors (M.Y.) is grateful for the financial assistance from the Special Postdoctoral Researcher Program of RIKEN. The numerical calculations were performed on the NEC SX-8 and SX-5 supercomputers at Yukawa Institute for Theoretical Physics, Kyoto University

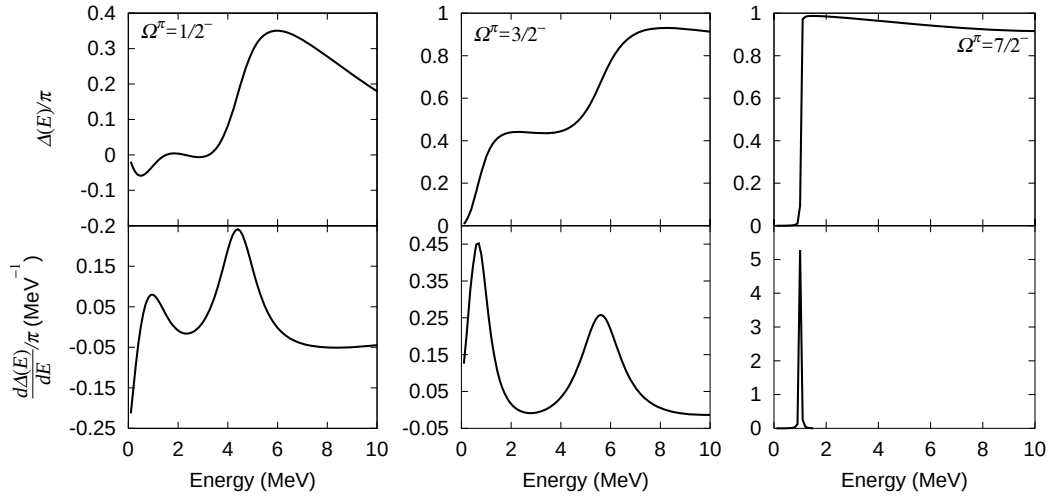

Fig. A.1. The eigenphase sum (upper panel) and its derivative (lower panel) for the $\Omega^\pi = 1/2^-, 3/2^-$ and $7/2^-$ states in ^{40}Mg are plotted as functions of energy.

and NEC SX-5 supercomputer at Research Center for Nuclear Physics, Osaka University.

A Eigenphase sum for single-particle resonance states

We examine properties of three single-particle states in the continuum, which play a key role in generating the low-lying excitations modes in ^{36,38,40}Mg. The resonance energy and width in a deformed potential can be estimated using the eigenphase sum $\Delta(E)$. It is defined in terms of the eigenvalues of the scattering matrix (S-matrix) as

$$(U^\dagger S U)_{aa'} = e^{2i\delta_a(E)}\delta_{aa'}, \quad \Delta(E) = \sum_a \delta_a(E). \tag{A.1}$$

We evaluate the eigenphase sum for three states following the procedure of Ref. [58]. The resonance energy and width are identified with the peak energy of $\frac{1}{\pi}d\Delta(E)/dE$ and its FWHM, respectively [59,60]. This evaluation is in good correspondence with another definition of the resonance; the Gamow state in a deformed potential [61] which represents the pole of the $S-$matrix in the complex momentum plane.

The result of this calculation, presented in Fig.A.1, indicates that the [301]1/2 and [312]3/2 states can be regarded as resonances with rather large widths; their energies are $0.53 - i0.46$ (MeV) and $0.42 - i0.33$ (MeV), respectively. On the other hand, the [303]7/2 state is evaluated as a narrow resonance with energy $0.44 - i0.0005$ (MeV). Obviously, the small width is due to its high centrifugal barrier.

References

[1] I. Tanihata (Ed), Nucl. Phys. A 693 (2001) Nos. 1, 2.

[2] H. Horiuchi, T. Otsuka, Y. Suzuki (Eds.), Prog. Theor. Phys. Suppl. No.142 (2001).

[3] K. Hagino, H. Horiuchi, M. Matsuo, I. Tanihata (Eds.), Prog. Theor. Phys. Suppl. No.146 (2002).

[4] I. Hamamoto, H. Sagawa, X. Z. Zhang, Phys. Rev. C 53 (1996) 765; ibid. 55 (1997) 2361; ibid. 56 (1997) 3121; ibid. 57 (1998) R1064; ibid. 64 (2001) 024313.

[5] I. Hamamoto, H. Sagawa, Phys. Rev. C 60 (1999) 064314; ibid. 62 (2000) 024319; ibid. 66 (2002) 044315.

[6] S. Shlomo, B. Agrawal, Nucl. Phys. A 722 (2003) 98c.

[7] M. Matsuo, Nucl. Phys. A 696 (2001) 371.

[8] K. Hagino, H. Sagawa, Nucl. Phys. A 695 (2001) 82.

[9] M. Bender, J. Dobaczewski, J. Engel, W. Nazarewicz, Phys. Rev. C 65 (2002) 054322.

[10] E. Khan, N. Sandulescu, M. Grasso, N. Van Giai, Phys. Rev. C 66 (2002) 024309.

[11] M. Yamagami, N. Van Giai, Phys. Rev. C 69 (2004) 034301.

[12] J. Terasaki, J. Engel, M. Bender, J. Dobaczewski, W. Nazarewicz, M. Stoitsov, Phys. Rev. C 71 (2005) 034310.

[13] M. Matsuo, K. Mizuyama, Y. Serizawa, Phys. Rev. C 71 (2005) 064326.

[14] D. Vretenar, N. Paar, P. Ring, G. A. Lalazissis, Nucl. Phys. A 692 (2001) 496

[15] N. Paar, P. Ring, T. Nikšić, D. Vretenar, Phys. Rev. C 67 (2003) 034312.

[16] N. Paar, T. Nikšić, D. Vretenar, P. Ring, Phys. Rev. C 69 (2004) 054303.

[17] N. Paar, T. Nikšić, D. Vretenar, P. Ring, Phys. Lett. B 606 (2005) 288.

[18] L. G. Cao, Z. Y. Ma, Phys. Rev. C 71 (2005) 034305.

[19] D. Vretenar, A. V. Afanasjev, G. A. Lalazissis, P. Ring, Phys. Rep. 409 (2005) 101.

[20] G. Giambrone, S. Scheit, F. Barranco, P. F. Bortignon, G. Colò, D. Sarchi, E. Vigezzi, Nucl. Phys. A 726 (2003) 3.

[21] S. Péru, J. F. Berger, P. F. Bortignon, Eur. Phys. J. A 26 (2005) 25.

[22] D. Sarchi, P. F. Bortignon, G. Coló, Phys. Lett. B 601 (2004) 27.

[23] M. Bender, P-H. Heenen, P-G. Reinhard, Rev. Mod. Phys. 75 (2003) 121.

[24] T. Nakatsukasa, K. Yabana, Phys. Rev. C 71 (2005) 024301.

[25] T. Inakura, H. Imagawa, Y. Hashimoto, S. Mizutori, M. Yamagami, K. Matsuyanagi, Nucl. Phys. A 768 (2006) 61

[26] R. H. Lemmer, M. Véneroni, Phys. Rev. 170 (1968) 883.

[27] A. Muta, J-I. Iwata, Y. Hashimoto, K. Yabana, Prog. Theor. Phys. 108 (2002) 1065.

[28] H. Imagawa, Y. Hashimoto, Phys. Rev. C 67 (2003) 037302.

[29] K. Yoshida, M. Yamagami, K. Matsuyanagi, Prog. Theor. Phys. 113 (2005) 1251.

[30] P. Urkedal, X. Z. Zhang, I. Hamamoto, Phys. Rev. C 64 (2001) 054304.

[31] R. Álvarez-Rodríguez, P. Sarriguren, E. Moya de Guerra, L. Pacearescu, A. Faessler, F. Šimkovic, Phys. Rev. C 70 (2004) 064309 and references therein.

[32] K. Hagino, N. Van Giai, H. Sagawa, Nucl. Phys. A 731 (2004) 264.

[33] A. Bulgac, Preprint No. FT-194-1980, Institute of Atomic Physics, Bucharest, 1980. [arXiv:nucl-th/9907088]

[34] J. Dobaczewski, H. Flocard, J. Treiner, Nucl. Phys. A 422 (1984) 103.

[35] R. Smolańczuk, J. Dobaczewski, Phys. Rev. C 48 (1993) R2166.

[36] J. Dobaczewski, I. Hamamoto, W. Nazarewicz, J. A. Sheikh, Phys. Rev. Lett. 72 (1994) 981.

[37] J. Dobaczewski, W. Nazarewicz, T. R. Werner, J. F. Berger, C. R. Chinn, J. Dechargé, Phys. Rev. C 53 (1996) 2809.

[38] K. Bennacuer, J. Dobaczewski, M. Płoszajczak, Phys. Rev. C 60 (1999) 034308.

[39] M. Yamagami, Phys. Rev. C 72 (2005) 064308.

[40] J. Terasaki, H. Flocard, P. -H. Heenen, P. Bonche, Nucl. Phys. A 621 (1997) 706.

[41] M. V. Stoitsov, J. Dobaczewski, W. Nazarewicz, S. Pittel, D. J. Dean, Phys. Rev. C 68 (2003) 054312.

[42] R. Rodoríguez-Guzmán, J. L. Egido, L. M. Robledo, Nucl. Phys. A 709 (2002) 201.

[43] E. Caurier, F. Nowacki, A. Poves, Nucl. Phys. A 742 (2004) 14.

[44] P.-G. Reinhard, D. J. Dean, W. Nazarewicz, J. Dobaczewski, J. A. Maruhn, M. R. Strayer, Phys. Rev. C 60 (1999) 014316 and references therein.

[45] K. Yoshida, M. Yamagami, K. Matsuyanagi, *Proc. Int. Conference on Finite Fermionic Systems – Nilsson Model 50 Years*, Lund, Sweden, 14-18 June, 2005, Phys. Scr. T 125 (2006) 45.

[46] E. Teran, V. E. Oberacker, A. S. Umar, Phys. Rev. C 67 (2003) 064314.

[47] G. F. Bertsch, H. Esbensen, Annu. Phys. 209 (1991) 327.

[48] J. Terasaki, P.-H. Heenen, P. Bonche, J. Dobaczewski, H. Flocard, Nucl. Phys. A 593 (1995) 1.

[49] J. Sauvage-Letessier, P. Quentin, H. Flocard, Nucl. Phys. A 370 (1981) 231.

[50] M. Bender, K. Rutz, P.-G. Reinhard, J. A. Maruhn, Eur. Phys. J. A 8 (2000) 59.

[51] T. Duguet, P. Bonche, P.-H. Heenen, Nucl. Phys. A 679 (2001) 427.

[52] M. Yamagami, K. Matsuyanagi, M. Matsuo, Nucl. Phys. A 693 (2001) 579.

[53] D. J. Rowe, *Nuclear Collective Motion*, (Methuen and Co. Ltd., 1970)

[54] E. Khan, N. Sandulescu, and N. Van Giai, Phys. Rev. C 71 (2005) R042801.

[55] S. Shlomo, G. F. Bertsch, Nucl. Phys. A 243 (1975) 507.

[56] A. Bohr, B. R. Motteleson, *Nuclear Structure*, vol. II (Benjamin, 1975; World Scientific 1998).

[57] A. Bohr, B. R. Motteleson, *Nuclear Structure*, vol. I (Benjamin, 1969; World Scientific 1998).

[58] K. Hagino, Nguyen Van Giai, Nucl. Phys. A 735 (2004) 55.

[59] M. Grasso, N. Sandulescu, Nguyen Van Giai, R. J. Liotta, Phys. Rev. C 64 (2001) 064321.

[60] A. Muta, T. Otsuka, Prog. Theor. Phys. Suppl. No.142 (2001) 355.

[61] K. Yoshida, K. Hagino, Phys. Rev. C 72 (2005) 064311.

[62] P. Curutchet, T. Vertse, R. J. Liotta, Phys. Rev. C 39 (1989) 1020.